Quantum Speed-Up in Collisional Battery Charging

Stella Seah,[1,*] Martí Perarnau-Llobet,[1] Géraldine Haack,[1] Nicolas Brunner,[1] and Stefan Nimmrichter[2,†]
[1]*Département de Physique Appliquée, Université de Genève, 1211 Genève, Switzerland*
[2]*Naturwissenschaftlich-Technische Fakultät, Universität Siegen, Siegen 57068, Germany*

(Received 11 May 2021; revised 1 July 2021; accepted 6 August 2021; published 31 August 2021)

We present a collision model for the charging of a quantum battery by identical nonequilibrium qubit units. When the units are prepared in a mixture of energy eigenstates, the energy gain in the battery can be described by a classical random walk, where both average energy and variance grow linearly with time. Conversely, when the qubits contain quantum coherence, interference effects buildup in the battery and lead to a faster spreading of the energy distribution, reminiscent of a quantum random walk. This can be exploited for faster and more efficient charging of a battery initialized in the ground state. Specifically, we show that coherent protocols can yield higher charging power than any possible incoherent strategy, demonstrating a quantum speed-up at the level of a single battery. Finally, we characterize the amount of extractable work from the battery through the notion of ergotropy.

DOI: 10.1103/PhysRevLett.127.100601

The development of thermodynamic protocols exploiting quantum effects like coherences and entanglement to outperform their classical counterparts has been a major focus in the field of quantum thermodynamics [1,2]. A simple scenario to explore this question is a *quantum battery*: a quantum system that receives or supplies energy [3–5]. Examples include simple qubit batteries [6,7], collective spins [8], interacting spin chains [9,10], and mechanical flywheels [11–13].

Alicki and Fannes developed the first quantum advantage in these devices: entangling operations over multiple batteries can extract more work than local operations [3]. Afterward, the relevance of entanglement for battery charging power was characterized in [7,14,15], while implementations were proposed based on collective superradiant coupling in cavity and waveguide QED setups [16–20]. Speed-ups due to many-body interactions were explored in [9,21–24] and theoretical bounds derived in [10]. Charging processes that exploit (or suffer from) dissipation [25–29], stabilization mechanisms [30–34], and the impact of energy fluctuations [35–40] have also been investigated.

Here, we explore the quantum advantage in charging a *single* battery, which arises from the quantum nature of the charging protocol. Any charging process involves auxiliary systems that provide the charge: a thermal engine [11,41,42], an external time-dependent field [4,7,15], a quantized light field [16–20], or more generally an out-of-equilibrium system [8]. We describe the charging process using a collision model [42–46], see Fig. 1. Collision models have proven useful to the understanding of equilibration and nonequilibrium dynamics [43–45,47,48], the impact of quantum coherence in thermodynamics [49,50], as well as strong coupling thermodynamics [51].

We find that energy coherences in the charging units generate interference effects in the battery. This leads to a fast spread of the battery's energy distribution, whose variance increases quadratically in time (instead of linear increase with classical units). The behavior is reminiscent of quantum random walks [52–54], which play a crucial role in the speed-up of quantum algorithms [55–57]. Specifically, we find that coherently prepared units can lead to faster charging than their classical counterparts for batteries prepared in the ground state. Notably, when charging power becomes the figure of merit, quantum protocols can overcome arbitrary classical ones. Finally, we study the efficiency of these charging processes, by comparing the ergotropy [58] in the battery with that of the charging units.

Model.—We consider a quantum battery with $N+1$ levels, Hamiltonian $\hat{H}_B = E\sum_0^N n|n\rangle\langle n|$, and lowering

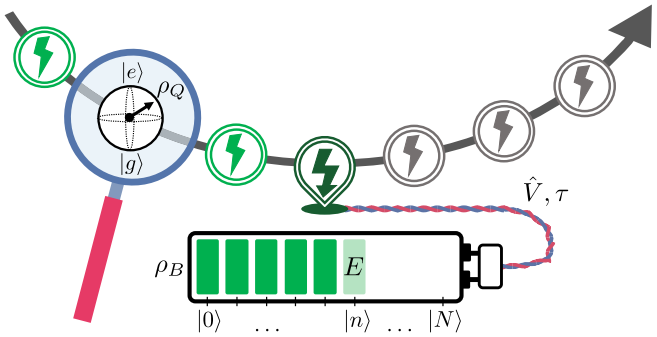

FIG. 1. Sketch of the collisional battery charging protocol. The battery is modeled as a uniform energy ladder with $N+1$ levels in steps of E. Its quantum state ρ_B receives energy "charge" from a stream of identical qubits prepared in the state ρ_Q, via the resonant exchange interaction $\hat{V}$ applied for a time τ.

operator $\hat{A} = \sum_1^N |n-1\rangle\langle n|$ [41,59]. The battery is charged by interacting with a sequence of *resonant* qubits with ground and excited states $|g\rangle, |e\rangle$, and bare Hamiltonian $\hat{H}_Q = E|e\rangle\langle e|$.

We consider the swap interaction $\hat{V} = \hbar g(\hat{\sigma}_+\hat{A} + \hat{\sigma}_-\hat{A}^\dagger)$ acting for a time τ at each charging step, which generates a thermal operation, $[\hat{V}, \hat{H}_B + \hat{H}_Q] = 0$ [60,61], characterized by a single parameter $\theta = g\tau$. The battery-qubit coupling thus does not require external work [62]. An arbitrary qubit state,

$$\rho_Q = q|g\rangle\langle g| + (1-q)|e\rangle\langle e| + c\sqrt{q(1-q)}(e^{i\alpha}|e\rangle\langle g| + \text{H.c.}), \tag{1}$$

with $q \in [0,1]$ the ground-state occupation, $\alpha \in [0, 2\pi]$ the phase, and $c \in [0,1]$ the degree of coherence contains an average energy $E(1-q)$, which is partly transferred to the battery via $\hat{V}$.

The transformation of the battery state $\rho_B \to \rho_B'$ after one charge step can be expressed via a Lindblad generator, $\Delta\rho_B = \rho_B' - \rho_B = \mathcal{L}\rho_B$. For a given q, we distinguish the two opposing cases of incoherent charging via diagonal qubit states ($c = 0$) and coherent charging via pure superposition states ($c = 1$). In the rotating frame with respect to $\hat{H}_B + \hat{H}_Q$, we get for $c = 0$ the generator

$$\mathcal{L}_{\text{inc}}\rho_B = \sin^2\theta\{q\mathcal{D}[\hat{A}]\rho_B + (1-q)\mathcal{D}[\hat{A}^\dagger]\rho_B\} + (1-\cos\theta)^2(q\mathcal{D}[|0\rangle\langle 0|]\rho_B + (1-q)\mathcal{D}[|N\rangle\langle N|]\rho_B), \tag{2}$$

where $\mathcal{D}[\hat{B}]\rho = \hat{B}\rho\hat{B}^\dagger - \{\hat{B}^\dagger\hat{B}, \rho\}/2$. The first line describes jumps up and down the energy ladder, conditioned on the qubit's ground (q) and excitation probabilities ($1-q$). This constitutes a random walk with an overall jump probability $p_\theta = \sin^2\theta$ and leads to an average energy change per charge step of

$$\text{tr}\{\hat{H}_B\mathcal{L}_{\text{inc}}\rho_B\} = vE + p_\theta E[q\langle 0|\rho_B|0\rangle - (1-q)\langle N|\rho_B|N\rangle]. \tag{3}$$

Here, $v = p_\theta(1-2q)$ denotes the (classical) dimensionless drift across the battery. Average energy growth ($v > 0$) requires population inversion, $q < 1/2$. For a finite battery, the jumps are terminated at the boundaries and complemented by dephasing of the boundary states, as described in the second line of (2): if no jump occurs, a ground-state (excited) qubit would learn that the battery is empty (full). The dephasing would destroy any initial energy coherence.

For $c = 1$, we get

$$\mathcal{L}_{\text{coh}}\rho_B = -i\sqrt{q(1-q)}\sin\theta\cos\theta[\hat{A}e^{-i\alpha} + \hat{A}^\dagger e^{i\alpha}, \rho_B] + \mathcal{D}[\sqrt{q}\sin\theta\hat{A} + ie^{i\alpha}\sqrt{1-q}(1-\cos\theta)|N\rangle\langle N|]\rho_B + \mathcal{D}[\sqrt{1-q}\sin\theta\hat{A}^\dagger + ie^{-i\alpha}\sqrt{q}(1-\cos\theta)|0\rangle\langle 0|]\rho_B. \tag{4}$$

The coherent generator (4) contains all incoherent terms with additional cross terms and an effective coherent driving Hamiltonian (first line). This driving term can generate interference effects in the case of strictly *partial* swaps ($\sin 2\theta \neq 0$). We identify the effective Rabi parameter

$$\Omega := 2\sqrt{q(1-q)}\sin\theta\cos\theta = \sqrt{q(1-q)}\sin 2\theta, \tag{5}$$

which quantifies the coherent speedup of battery charging. Other c values would result in a mixture of the two generators, $\mathcal{L}\rho_B = c\mathcal{L}_{\text{coh}}\rho_B + (1-c)\mathcal{L}_{\text{inc}}\rho_B$.

Incoherent charging.—We first consider a classical charging protocol ($c = 0$). From (2), the battery state then remains diagonal, fully characterized by the populations $P(n,k) = \langle n|\rho_B(k)|n\rangle$ after interaction with the kth qubit. In the regime where the battery does not populate the boundary states $|0\rangle$ and $|N\rangle$, we obtain a discrete three-branch random walk with an update rule

$$P(n,k+1) = (1-p_\theta)P(n,k) + p_\theta(1-q)P(n-1,k) + p_\theta q P(n+1,k), \tag{6}$$

valid for $0 < n < N$. The variable for the number of jumps up-down or no jumps after k interactions, $\mathbf{X} = \{X_+, X_-, X_0\}$, follows a trinomial distribution with probabilities $\mathbf{p} = \{p_\theta(1-q), p_\theta q, 1-p_\theta\}$ [63]. The mean and variance of charge n (energy in units E) grow linearly in time,

$$\bar{n}(k) = \bar{n}(0) + vk, \qquad \Delta n^2(k) = \Delta n^2(0) + (p_\theta - v^2)k, \tag{7}$$

with $\bar{n}(k) = \sum_n nP(n,k)$ and $\Delta n^2(k) = \sum_n n^2P(n,k) - \bar{n}(k)^2$. Taking $k \gg 1$, the trinomial distribution has two natural limits. For small jump probabilities ($p_\theta \ll 1$) and finite kp_θ, the number of jumps up or down obey a Poisson distribution with mean $kp_\pm$ [64,65]. Conversely, for large k and moderate $p_\theta \not\approx 0, 1$, $\mathbf{X}$ follows a Gaussian distribution in accordance with the central limit theorem [66]. The battery populations eventually converge to $P(n,\infty) \propto (1-q)^n/q^n$, the fixed point of (6). It amounts to a Gibbs state at an effective (negative) qubit temperature defined by $e^{-E/k_BT} = (1-q)/q$; this follows by noting that the product Gibbs state $\rho_Q \otimes \rho_B \propto e^{-(\hat{H}_Q + \hat{H}_B)/k_BT}$ is

invariant under $\hat{V}$ while population inversion ($q < 1/2$) implies $T < 0$.

Coherent charging and quantum signatures.—Now, instead of using classical population-inverted states to charge the battery, consider qubits prepared in pure superposition states with the same occupation q. They have the same mean energy but a higher purity, which can be interpreted as a thermodynamic resource [49,50]. Since $\hat{V}$ is invariant under rotation about the z axis, we set the qubit phase $\alpha = 0$ without loss of generality.

Ignoring boundary effects, one can show that a bimodal energy distribution emerges. The two branches simultaneously progress down and up the energy ladder with increasing k [66]. For an initially pure battery state $|n_0\rangle$ and sufficiently large k ($n_0 - k > 0$ and $n_0 + k < N$), the two branches have energy peaks at approximately

$$n_\pm \approx n_0 + (v \pm c\Omega)k. \tag{8}$$

The coherent driving thus speeds up (and slows down) each peak by $c\Omega$, resulting in the same mean energy increase as in the incoherent case (7). However, the energy variance now grows quadratically with k, $\Delta n^2(k) \approx (p_\theta - v^2)k + c^2\Omega^2 k(k-1)/2$, which can be seen as a genuine quantum signature.

Exemplary snapshots of the battery's energy distribution with k are depicted in Fig. 2(a) for coherent (red) and incoherent charging (black). The incoherent case is well described by Gaussians whose mean values (black-dotted lines) move according to (7). The red-dotted lines mark the approximate peak positions (8) for the coherent case, which agree with the actual distribution maxima. Note that the average energy $\bar{n}(k)$ is the same in both cases as long as the boundaries are not hit. Once this happens, the quantum wave is reflected, whereas the classical distribution approaches the inverse Gibbs state.

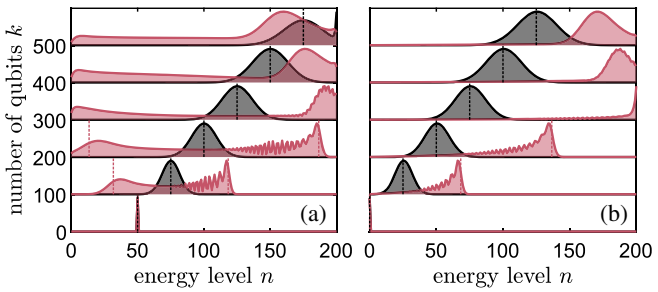

FIG. 2. Energy distributions of a battery of size $N = 200$ charged by k incoherent (black) and coherent (red) qubits with $q = 1/4$ and $\theta = \pi/4$. All curves are rescaled to the same maximum. In (a), the battery is initialized in the pure, partially charged state $|n_0 = 50\rangle$, whereas in (b), the battery is initialized in the zero-charge state $|0\rangle$. The dotted black and red vertical lines mark the approximate average charge according to (7) and the approximate peak positions (8) for incoherent and coherent qubits, respectively, for $\bar{n} < 200$.

Quantum advantage for empty batteries.—At first sight, the previous considerations suggest that quantum coherence is detrimental for battery charging: coherent qubits provide at most the same average energy to the battery as incoherent ones, but with a larger variance. The situation drastically changes when the battery is initially empty ($n_0 = 0$). Now the charge distribution comprises only a single forward-propagating peak, see Fig. 2(b). Even though our analytic random-walk model no longer applies, we verify numerically that the peak is still situated close to n_+ from (8), which climbs up the ladder at a 73% faster rate than the incoherent Gaussian for $q = 0.25$. Coherence results in interference effects and directly attributes to the speed-up by $c\Omega$. In fact, both purity and coherence can be seen as independent resources for this task: a higher purity leads to a higher (classical) drift velocity $v = p_\theta(1 - 2q)$, whereas coherence adds an additional contribution $c\Omega$ to the velocity [see Eq. (8)].

We compare the energy growth of incoherent and coherent protocols in Fig. 3(a) for $q = 0.25$; and in (b) for the more distinctive case $q = 0.49$. Far below the fully charged state, coherent charging is always more advantageous. However, once the maximum charge is reached, we see a drop in energy due to reflection at the boundary $n = N$. The number of coherent steps from empty to maximum battery charge is therefore

$$k_{\text{est}} \approx \left\lfloor \frac{N}{c\Omega + v} \right\rfloor. \tag{9}$$

For Fig. 3, this amounts to (a) $k_{\text{est}} \approx 292$ and (b) 392, in good agreement with the depicted maxima. Beyond this point, the quantum protocol loses its advantage, whereas the incoherent protocol continues to charge. This suggests a hybrid protocol in which the battery is charged coherently until $k \approx k_{\text{est}}$ to exploit the quantum speedup, then incoherently until the battery reaches an inverted Gibbs state.

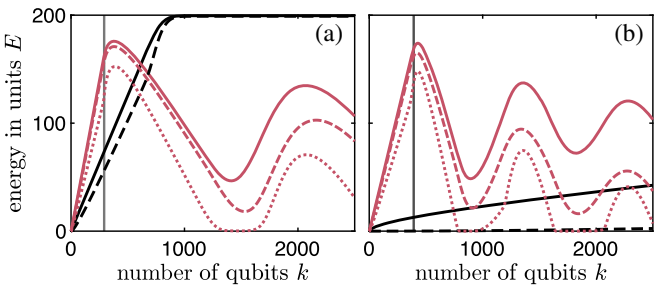

FIG. 3. Energy (solid) and ergotropy (dashed) for incoherent (black) and coherent (red) charging of a battery of $N = 200$ with k qubits. Here, (a) matches Fig. 2(b) with $q = 0.25$ and $n_0 = 0$ while (b) corresponds to $q = 0.49$. The dotted line shows the ergotropy associated to the dephased battery state, i.e., only the energy populations. The vertical lines mark the theoretical k_{est}.

Focusing on $k < k_{\mathrm{est}}$, the quantum advantage can be quantified by the ratio between incoherent ($c = 0$) and coherent ($c = 1$) energy charging rate:

$$\mathcal{A}(k) = \frac{\bar{n}_{c=1}(k) - \bar{n}_{c=1}(k-1)}{\bar{n}_{c=0}(k) - \bar{n}_{c=0}(k-1)}. \tag{10}$$

Here, the subindex in $\bar{n}(k)$ distinguishes both cases. There is a quantum advantage if $\mathcal{A} > 1$ for some k, q, and θ. In the regime $N > k \gg 1$, we obtain an upper bound on $\mathcal{A}$ by noting that the increment of $\bar{n}_{c=1}$ is upper bounded by the peak velocity $v + \Omega$, whereas the classical increment is, for the most part, given by v,

$$\mathcal{A} \lesssim 1 + \frac{\Omega}{v} = 1 + \frac{2\sqrt{q(1-q)}}{(1-2q)\tan\theta}. \tag{11}$$

It can be verified numerically that $\mathcal{A}$ is always above 70% of this bound. Moreover, the quantum advantage diverges for $q \to 1/2$ and for $\theta \ll 1$. This can be understood by noting that for $q \approx 1/2$, incoherent charging vanishes while coherent charging is still possible. For short interactions ($\theta \ll 1$), the coherent driving term in (4) is first order in θ, while the classical charging terms are of second order.

Ergotropy and charging efficiency.—Because of inevitable energy fluctuations, not all energy stored in the battery is useful work. This effect is well captured by the notion of ergotropy [1,58], which characterizes the maximum amount of useful energy as the part that can be extracted by means of a deterministic unitary operation. The unitary brings the battery to a passive state [58,69,70], given by the energy mixture $\pi_B = \sum_0^N r_n |n\rangle\langle n|$ with $\{r_n\}$ the eigenvalues of the initial state in *descending* order.

Figure 3 shows the ergotropy and average energy of the battery. When charged by coherent qubits, the battery stores useful energy in two ways: by populating higher energies and building up energy coherences. We distinguish the two by considering the residual ergotropy from a dephased battery state in the energy basis (dotted). In fact, most useful energy is contained in the energy profile during the charging of an initially empty battery until it reaches maximum charge. In the longtime limit, however, ergotropy will approach comparatively low values almost entirely contained in coherences: for $c = 1$ in Figs. 3(a) and 3(b), the ergotropy converges to $51E$ and $14E$ at $k \to \infty$, respectively, while the dephased-state ergotropy converges to $1E$ and $0.2E$.

Ergotropy provides a natural way to define the charging efficiency without a reference temperature [66]. For k qubits, each with ergotropy $\mathcal{E}_Q = E[1 - 2q + \sqrt{(1-2q)^2 + 4c^2 q(1-q)}]/2$, we define the efficiency as the ratio of stored ergotropy over total ergotropy input, $\eta(k) = \mathcal{E}_B(k)/k\mathcal{E}_Q$. Note that $\eta(k) \leq 1$ for energy-preserving interactions [37].

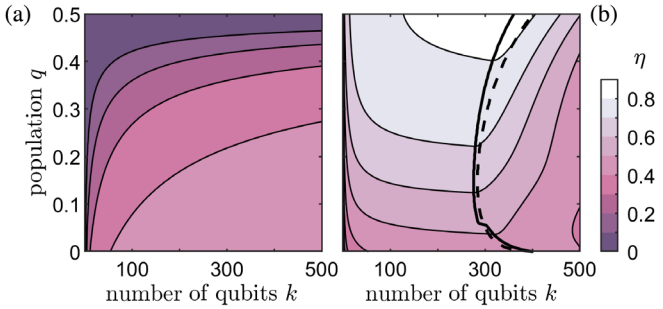

FIG. 4. (a) Incoherent and (b) coherent charging efficiency η for a battery of size $N = 200$ initialized in the zero-charge state for different k and q. Here, we consider $\theta = \pi/4$ where interference effects are the strongest. The solid line in (b) marks the number of qubits that maximizes η for a given q value, while the dashed line marks the estimated k_{est} in (9).

Figure 4 shows the (a) incoherent and (b) coherent charging efficiency as a function of k and q. Coherent ergotropy transfer can reach more than 80% maximum efficiency at intermediate qubit numbers k, indicated by the solid curve in Fig. 4(b) and compared against k_{est} (dashed). The efficiency drops for greater k values after reflection at the full-charge state $|N\rangle$. Incoherent charging slows down approaching the inverted Gibbs state.

Quantum advantage in power.—The previous considerations show that quantum coherence can be exploited to enhance battery charging and its efficiency given a set of k qubits with fixed interaction θ. However, the energy $\bar{n}(k)E$ charged into the battery would be maximum for perfect population inversion ($q \to 0$), and charging efficiency would reach $\eta(k) = 1$ for full swaps ($\theta = \pi/2$). Crucially, this best-case scenario does not require quantum coherence, which raises the natural question: can we find a quantum advantage against arbitrary classical protocols? Remarkably, the answer is affirmative when charging *power* is the figure of merit and *time* the only constraint.

Starting with an empty battery [$\bar{n}(0) = 0$], the average charging power of k qubits, $\mathcal{P}(k) = gE\bar{n}(k)/k\theta = E\bar{n}(k)/t$, quantifies the gain in average battery energy over the charging time $t = k\theta/g$. We shall maximize $\mathcal{P}$ over k and q at *fixed* t. For incoherent probes, power decreases monotonically with q, and the optimal strategy is hence obtained for pure excited qubit states at $q = 0$. A straightforward calculation yields the fundamental upper bound for incoherent charging, $\mathcal{P}_{c=0}^{\max} \approx 0.62gE$ attained at $\theta_{\max} \approx 1.17$.

Coherent probes can overcome this bound, see Fig. 5, which singles out coherence (and not purity) as the relevant thermodynamic resource causing the advantage. That is, coherent qubits ($c \neq 0$) can outperform arbitrary incoherent strategies, including pure excited qubits ($q = 0$).

The optimal coherent strategy involves taking $q = 1/2$ and the limit of $\theta \to 0$ and $k \to \infty$, which caps the velocity of the fast-moving peak in (8) at $\Omega k/t \to g$ (solid line). In this case, the power is initially smaller, but after a transient

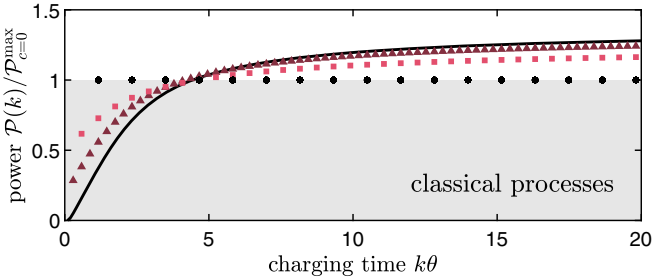

FIG. 5. Quantum advantage in terms of power normalized to the best incoherent charging protocol (circles), which uses a sequence of excited qubits ($q = 0$) with interaction parameter $\theta_{\max}$. The gray region bounds all classical processes. The solid curve represents the continuous quantum limit using $k \to \infty$ coherent qubits at $q = 1/2$. The squares and triangles represent coherent protocols for finite qubits with $q = 0.26$ and 0.38 interacting over $\theta = \theta_{\max}/2$ and $\theta_{\max}/4$, respectively. The chosen q values yield optimal power in the regime of $N > k \gg 1$.

buildup of quantum coherence, it overcomes the incoherent bound (circles) and hits $\mathcal{P}_{c=1}^{\max} \approx 0.85gE = 1.37\mathcal{P}_{c=0}^{\max}$ at $1 \ll k < N$. In practice, one can already achieve a significant coherent power enhancement with finite qubits (triangles and squares). Importantly, the advantage remains in terms of ergotropy. At $k\theta = 20$, the ergotropy charging power still exceeds the classical bound, and amounts to 91% and 96% of $\mathcal{P}_{c=1}(k)$ for $\theta_{\max}/2$ and $\theta_{\max}/4$, respectively. In the limit $q = 1/2$ and $\theta \to 0$, the ergotropy matches exactly the energy gain since the battery evolves almost unitarily, building up energy in its coherences through $\hat{A} + \hat{A}^\dagger$ according to (4).

Conclusions.—We proposed a collision model for quantum battery charging, in which identical qubits (charging units) transfer energy to a finite energy ladder (battery). We compared classical to quantum charging protocols where the units are prepared in a mixture or superposition state, respectively. We found that quantum protocols can yield a higher power than arbitrary classical strategies, thus providing a clear advantage at the level of a single battery. This complements previous examples of collective quantum speed-ups [4,5]. Our analysis also highlights a connection between quantum thermodynamics and quantum random walks [52–54]. The formalism behind is, however, different: in quantum random walks a single coin becomes entangled with the walker, whereas here interference effects in the walker (battery) are created through partial collision processes with numerous coins (units). Future work could further reveal the connection between both frameworks and exploit quantum walklike features in thermodynamic protocols.

S. S. and N. B. acknowledge funding from Swiss National Science Foundation (NCCR SwissMAP). M. P.-L. and G. H. acknowledge funding from Swiss National Science Foundation through an Ambizione Grant No. PZ00P2-186067 and a starting Grant No. PRIMA PR00P2-179748, respectively.

*stella.seah@unige.ch
†stefan.nimmrichter@uni-siegen.de

[1] J. Goold, M. Huber, A. Riera, L. del Rio, and P. Skrzypczyk, J. Phys. A **49**, 143001 (2016).
[2] S. Vinjanampathy and J. Anders, Contemp. Phys. **57**, 545 (2016).
[3] R. Alicki and M. Fannes, Phys. Rev. E **87**, 042123 (2013).
[4] F. Campaioli, F. A. Pollock, and S. Vinjanampathy, in *Fundamental Theories of Physics* (Springer International Publishing, New York, 2018), pp. 207–225.
[5] S. Bhattacharjee and A. Dutta, arXiv:2008.07889.
[6] M. Horodecki and J. Oppenheim, Nat. Commun. **4**, 2059 (2013).
[7] F. C. Binder, S. Vinjanampathy, K. Modi, and J. Goold, New J. Phys. **17**, 075015 (2015).
[8] G. M. Andolina, M. Keck, A. Mari, V. Giovannetti, and M. Polini, Phys. Rev. B **99**, 205437 (2019).
[9] T. P. Le, J. Levinsen, K. Modi, M. M. Parish, and F. A. Pollock, Phys. Rev. A **97**, 022106 (2018).
[10] S. Julià-Farré, T. Salamon, A. Riera, M. N. Bera, and M. Lewenstein, Phys. Rev. Research **2**, 023113 (2020).
[11] A. Levy, L. Diósi, and R. Kosloff, Phys. Rev. A **93**, 052119 (2016).
[12] A. Roulet, S. Nimmrichter, J. M. Arrazola, S. Seah, and V. Scarani, Phys. Rev. E **95**, 062131 (2017).
[13] S. Seah, S. Nimmrichter, and V. Scarani, New J. Phys. **20**, 043045 (2018).
[14] K. V. Hovhannisyan, M. Perarnau-Llobet, M. Huber, and A. Acín, Phys. Rev. Lett. **111**, 240401 (2013).
[15] F. Campaioli, F. A. Pollock, F. C. Binder, L. Céleri, J. Goold, S. Vinjanampathy, and K. Modi, Phys. Rev. Lett. **118**, 150601 (2017).
[16] D. Ferraro, M. Campisi, G. M. Andolina, V. Pellegrini, and M. Polini, Phys. Rev. Lett. **120**, 117702 (2018).
[17] D. Ferraro, G. M. Andolina, M. Campisi, V. Pellegrini, and M. Polini, Phys. Rev. B **100**, 075433 (2019).
[18] G. M. Andolina, M. Keck, A. Mari, M. Campisi, V. Giovannetti, and M. Polini, Phys. Rev. Lett. **122**, 047702 (2019).
[19] F. Pirmoradian and K. Mølmer, Phys. Rev. A **100**, 043833 (2019).
[20] J. Monsel, M. Fellous-Asiani, B. Huard, and A. Auffèves, Phys. Rev. Lett. **124**, 130601 (2020).
[21] D. Rossini, G. M. Andolina, and M. Polini, Phys. Rev. B **100**, 115142 (2019).
[22] D. Rossini, G. M. Andolina, D. Rosa, M. Carrega, and M. Polini, Phys. Rev. Lett. **125**, 236402 (2020).
[23] D. Rosa, D. Rossini, G. M. Andolina, M. Polini, and M. Carrega, J. High Energy Phys. 11 (2020) 67.
[24] S. Ghosh, T. Chanda, and A. Sen(De), Phys. Rev. A **101**, 032115 (2020).
[25] F. Barra, Phys. Rev. Lett. **122**, 210601 (2019).
[26] D. Farina, G. M. Andolina, A. Mari, M. Polini, and V. Giovannetti, Phys. Rev. B **99**, 035421 (2019).
[27] F. H. Kamin, F. T. Tabesh, S. Salimi, F. Kheirandish, and A. C. Santos, New J. Phys. **22**, 083007 (2020).
[28] K. V. Hovhannisyan, F. Barra, and A. Imparato, Phys. Rev. Research **2**, 033413 (2020).
[29] F. T. Tabesh, F. H. Kamin, and S. Salimi, Phys. Rev. A **102**, 052223 (2020).

[30] A. C. Santos, B. Çakmak, S. Campbell, and N. T. Zinner, Phys. Rev. E **100**, 032107 (2019).
[31] S. Gherardini, F. Campaioli, F. Caruso, and F. C. Binder, Phys. Rev. Research **2**, 013095 (2020).
[32] J. Q. Quach and W. J. Munro, Phys. Rev. Applied **14**, 024092 (2020).
[33] A. C. Santos, A. Saguia, and M. S. Sarandy, Phys. Rev. E **101**, 062114 (2020).
[34] M. T. Mitchison, J. Goold, and J. Prior, Quantum **5**, 500 (2021).
[35] N. Friis and M. Huber, Quantum **2**, 61 (2018).
[36] E. McKay, N. A. Rodríguez-Briones, and E. Martín-Martínez, Phys. Rev. E **98**, 032132 (2018).
[37] M. Perarnau-Llobet and R. Uzdin, New J. Phys. **21**, 083023 (2019).
[38] L. P. García-Pintos, A. Hamma, and A. del Campo, Phys. Rev. Lett. **125**, 040601 (2020).
[39] A. Crescente, M. Carrega, M. Sassetti, and D. Ferraro, New J. Phys. **22**, 063057 (2020).
[40] F. Caravelli, G. Coulter-De Wit, L. P. García-Pintos, and A. Hamma, Phys. Rev. Research **2**, 023095 (2020).
[41] N. Brunner, N. Linden, S. Popescu, and P. Skrzypczyk, Phys. Rev. E **85**, 051117 (2012).
[42] E. Bäumer, M. Perarnau-Llobet, P. Kammerlander, H. Wilming, and R. Renner, Quantum **3**, 153 (2019).
[43] V. Scarani, M. Ziman, P. Štelmachovič, N. Gisin, and V. Bužek, Phys. Rev. Lett. **88**, 097905 (2002).
[44] L. Bruneau, A. Joye, and M. Merkli, J. Math. Phys. (N.Y.) **55**, 075204 (2014).
[45] D. Grimmer, D. Layden, R. B. Mann, and E. Martín-Martínez, Phys. Rev. A **94**, 032126 (2016).
[46] P. Strasberg, G. Schaller, T. Brandes, and M. Esposito, Phys. Rev. X **7**, 021003 (2017).
[47] S. Seah, S. Nimmrichter, and V. Scarani, Phys. Rev. E **99**, 042103 (2019).
[48] M. Cattaneo, G. De Chiara, S. Maniscalco, R. Zambrini, and G. L. Giorgi, Phys. Rev. Lett. **126**, 130403 (2021).
[49] F. L. S. Rodrigues, G. De Chiara, M. Paternostro, and G. T. Landi, Phys. Rev. Lett. **123**, 140601 (2019).
[50] K. Hammam, Y. Hassouni, R. Fazio, and G. Manzano, New J. Phys. **23**, 043024 (2021).
[51] P. Strasberg, Phys. Rev. Lett. **123**, 180604 (2019).
[52] A. Ambainis, E. Bach, A. Nayak, A. Vishwanath, and J. Watrous, in *Proceedings of the Thirty-Third Annual ACM Symposium on Theory of Computing, STOC '01* (Association for Computing Machinery, New York, 2001), p. 3749.
[53] J. Kempe, Contemp. Phys. **44**, 307 (2003).
[54] E. Bach, S. Coppersmith, M. P. Goldschen, R. Joynt, and J. Watrous, J. Comput. Syst. Sci. **69**, 562 (2004).
[55] A. M. Childs, R. Cleve, E. Deotto, E. Farhi, S. Gutmann, and D. A. Spielman, in *Proceedings of the Thirty-Fifth Annual ACM Symposium on Theory of Computing, STOC '03* (Association for Computing Machinery, New York, 2003), p. 5968.
[56] V. M. Kendon, Phil. Trans. R. Soc. A **364**, 3407 (2006).
[57] A. M. Childs, L. J. Schulman, and U. V. Vazirani, in *Proceedings of the 48th Annual IEEE Symposium on Foundations of Computer Science (FOCS'07)* (IEEE, New York, 2007), pp. 395–404, https://ieeexplore.ieee.org/document/4389510.
[58] A. E. Allahverdyan, R. Balian, and T. M. Nieuwenhuizen, Europhys. Lett. **67**, 565 (2004).
[59] P. Erker, M. T. Mitchison, R. Silva, M. P. Woods, N. Brunner, and M. Huber, Phys. Rev. X **7**, 031022 (2017).
[60] F. G. S. L. Brandão, M. Horodecki, J. Oppenheim, J. M. Renes, and R. W. Spekkens, Phys. Rev. Lett. **111**, 250404 (2013).
[61] F. Brandão, M. Horodecki, N. Ng, J. Oppenheim, and S. Wehner, Proc. Natl. Acad. Sci. U.S.A. **112**, 3275 (2015).
[62] F. Barra, Sci. Rep. **5**, 14873 (2015).
[63] J. Franke, W. K. Härdle, and C. M. Hafner, Stochastic processes in discrete time, in *Statistics of Financial Markets: An Introduction* (Springer Berlin Heidelberg, Berlin, Heidelberg, 2015), pp. 49–58.
[64] G. F. Lawler and V. Limic, *Random Walk: A Modern Introduction*, Cambridge Studies in Advanced Mathematics (Cambridge University Press, Cambridge, England, 2010).
[65] P. Deheuvels and D. Pfeifer, J. Multivariate Anal. **25**, 65 (1988).
[66] See Supplemental Material at http://link.aps.org/supplemental/10.1103/PhysRevLett.127.100601 for details on the battery state and the differences in efficiency computed from the qubits' ergotropy and free energy difference, which includes Refs. [67–68].
[67] P. Skrzypczyk, A. J. Short, and S. Popescu, Nat. Commun. **5**, 4185 (2014).
[68] M. N. Bera, A. Riera, M. Lewenstein, Z. B. Khanian, and A. Winter, Quantum **3**, 121 (2019).
[69] W. Pusz and S. L. Woronowicz, Commun. Math. Phys. **58**, 273 (1978).
[70] A. Lenard, J. Stat. Phys. **19**, 575 (1978).